






Article

Effect of Doping Element and Electrolyte's pH on the Properties of Hydroxyapatite Coatings Obtained by Pulsed Galvanostatic Technique

Elena Ungureanu ¹, Diana Maria Vranceanu ^{1,*}, Alina Vladescu ^{2,3}, Anca Constantina Parau ², Mihai Tarcolea ¹ and Cosmin Mihai Cotrut ^{1,*}

- ¹ Faculty of Materials Science and Engineering, University Politehnica of Bucharest, 313 Spl. Independentei, 060042 Bucharest, Romania; ungureanu.elena14@yahoo.com (E.U.); mihai.tarcolea@upb.ro (M.T.)
 - ² Department for Advanced Surface Processing and Analysis by Vacuum Technologies, National Institute of Research and Development for Optoelectronics—INOE 2000, 409 Atomistilor St., 77125 Magurele, Romania; alinava@inoe.ro (A.V.); anca.parau@inoe.ro (A.C.P.)
 - ³ Physical Materials Science and Composite Materials Centre, Research School of Chemistry & Applied Biomedical Sciences, National Research Tomsk Polytechnic University, Lenin Avenue 43, 634050 Tomsk, Russia
- * Correspondence: diana.vranceanu@upb.ro (D.M.V.); cosmin.cotrut@upb.ro (C.M.C.)

Abstract: Hydroxyapatite (HAp) is the most widely used calcium phosphate as a coating on metal implants due to its biocompatibility and bioactivity. The aim of this research is to evaluate the effect of the pH's electrolyte and doping element on the morphology, roughness, chemical, and phasic composition of hydroxyapatite-based coatings obtained by pulsed galvanostatic electrochemical deposition. As doping elements, both Sr and Ag were selected due to their good osseointegrative character and antibacterial effect, respectively. The electrolytes were prepared at pH 4 and 5, in which specific concentrations of Sr, Ag, and Sr + Ag were added. In terms of morphology, all coatings consist in ribbon-like crystals, which at pH 5 appear to be a little larger. Addition of Sr did not affect the morphology of HAp, while Ag addition has led to the formation of flower-like crystals agglomeration. When both doping elements were added, the flowers like agglomerations caused by the Ag have diminished, indicating the competition between Sr and Ag. X-Ray Diffraction analysis has highlighted that Sr and/or Ag have successfully substituted the Ca in the HAp structure. Moreover, at higher pH, the crystallinity of all HAp coatings was enhanced. Thus, it can be said that the electrolyte's pH enhances to some extent the properties of HAp-based coatings, while the addition of Sr and/or Ag does not negatively impact the obtained features of HAp, indicating that by using pulsed galvanostatic electrochemical deposition, materials with tunable features dictated by the function of the coated medical device can be designed.

Keywords: electrolyte pH; silver; strontium; electrochemical deposition; coatings



Citation: Ungureanu, E.; Vranceanu, D.M.; Vladescu, A.; Parau, A.C.; Tarcolea, M.; Cotrut, C.M. Effect of Doping Element and Electrolyte's pH on the Properties of Hydroxyapatite Coatings Obtained by Pulsed Galvanostatic Technique. *Coatings* **2021**, *11*, 1522. <https://doi.org/10.3390/coatings11121522>

Academic Editor: Simona Liliana Iconaru

Received: 24 November 2021

Accepted: 7 December 2021

Published: 10 December 2021

Publisher's Note: MDPI stays neutral with regard to jurisdictional claims in published maps and institutional affiliations.



Copyright: © 2021 by the authors. Licensee MDPI, Basel, Switzerland. This article is an open access article distributed under the terms and conditions of the Creative Commons Attribution (CC BY) license (<https://creativecommons.org/licenses/by/4.0/>).

1. Introduction

In the past years, the use of implants has grown considerably, driven by ageing of populations and the desire of the patients to maintain the same level of activity and quality of life [1].

Among the metallic biomaterials, titanium is the most used due to its excellent properties such as the modulus of elasticity close to that of bone, biocompatibility, and excellent corrosion resistance, being considered the “gold standard” [2,3]. Titanium, due to its bioinert character does not favor the formation of a direct connection with the hard tissue nor the initiation of the bone remodeling mechanism in the early stages after implantation [4].

Imparting multifunctionality of bioinert metals such as Ti and its alloys is generally achieved through surface modification techniques [5], such as coating the metallic biomaterials with bioactive ceramics and/or polymers to improve their osseointegration and bioactivity [6].

Hydroxyapatite (HAp) is a calcium phosphate-based ceramic that is found in the structure of hard tissues along with collagen and minerals [7]. Due to its resemblance to its natural homologue, HAp can be doped with a large variety of ions such as Mg, Sr, Zn, Mn, and Si found in the structure of hard tissues [8,9].

Among these ions, strontium (Sr) can be found, which according to the literature [10], is an important element that facilitates the growth of new bone tissue, while reducing bone resorption. Both in vitro and in vivo studies have indicated that the presence of Sr^{2+} increases the number of osteoblasts, reduces the number and activity of osteoclast cells, and improves the bone tissue growth [11,12]. Consequently, Sr^{2+} is now considered a potential enhancer of bone implants [13].

In addition to optimizing the mechanical and chemical compatibilities, another important aspect is to obtain modified surfaces capable of guaranteeing a prolonged release of active substances in a quantity sufficient to destroy bacteria, without inducing a negative response from the host organism [14,15]. Thus, considerable efforts are being made in this direction, by developing materials that can support not only the bioactive character and osseointegration, but also offer at the same time a proper antibacterial effect, and becoming so more effective [16,17]. Through addition and usage of antibacterial elements, the post-surgery inflammation process can be controlled and/or even overcome, improving so the patient comfort by reducing the surgical traumas or the therapeutical treatments.

Thus, the deposition of HAp-based coatings-doped antibacterial elements, such as silver ion (Ag^+), zinc ion (Zn^{2+}), copper ion (Cu^{2+}), etc., represent a viable route for postoperative prevention and intraoperative treatment of infections associated with implants.

According to a study performed by Chen et al. [18] it was shown that the silver ions released from the Ag-doped HAp coatings in synthetic body fluid (SBF) solution was initially higher (in the first few days) and slower after 14 days. It was also highlighted that the release rate was directly proportional to the silver content in the layers. In a similar study conducted by Sandukas et al. [19], it has been shown that the Ag-HAp coatings with a lower silver content (1.1 wt.%) had the highest number of osteoblast cells on the surface, while the ones with 6.59 wt.% had a negative effect on cell proliferation and attachment, indicating that a too high silver concentration induces cytotoxicity. Therefore, it can be said that selection of the optimum Ag concentration for doping of the HAp-based coating is of crucial importance, as the use of too much can lead to cellular apoptosis [20]. In the study of Gent et al. [21], it was stated that co-substitution of Sr in Ag-HAp can alleviate the adverse effects of Ag and promote cellular viability. Similar findings have also been presented in another study [22], in which calcium phosphate (CaP) coatings co-doped with Sr and Ag showed a good biological activity and optimal antimicrobial properties. In consequence, one way to offset the negative effects of Ag is to add another element, such as Sr [23].

Several deposition techniques can be used to functionalize metallic substrate, especially Ti-based ones. Among these deposition techniques, the following can be found: magnetron sputtering [15], pulsed laser deposition [24], plasma spray [25], sol-gel [26], electrophoretic [27] and electrochemical deposition [28]. Of all these techniques, electrochemical deposition is widely used for coating titanium and its alloys used in biomedical applications. The deposition of hydroxyapatite by electrochemical methods is a rapid process with low costs, offering the possibility to coat surfaces with complex geometries, with uniform layers [29–31]. Another advantage of this technique is that the properties of the coatings can be controlled by changing the deposition parameters (e.g., deposition temperature, deposition technique, electrolyte's concentration and pH) [32,33]. The electrolyte's pH is the parameter on which the kinetics of the deposition reactions depend. Thus, a higher value of the electrolyte's pH leads to the release of a smaller amount of hydrogen, obtaining more uniform and compact layers [31].

Aim of this research is to develop suitable approaches for Sr and Ag single-doped and co-doped hydroxyapatite-based coatings on Ti substrate, through pulsed galvanostatic deposition technique, without any additional treatments (i.e., high temperature treatments

or alkaline treatment). To the best of our knowledge, there are only a few research on the Sr and Ag co-doped hydroxyapatite coatings obtained through electrochemical deposition [23,34].

To achieve this goal, different pH values of 4 and 5 were used, since a pH value higher than 4.5 leads to obtaining coatings with high crystallinity [35,36]. Besides this, the concentration of electrolytes used does not allow to modify the electrolyte's pH at values higher than 5. Any attempt to further increase the pH leads to the formation of insoluble ionic solid (precipitate) in the electrolyte. According to the literature [37–39], if the pH of the electrolyte is lower than 4.5, other phases are obtained unless a high current density or high deposition temperature is applied.

2. Materials and Methods

2.1. Coating Preparation

The undoped and doped HAp-based coatings with Sr and/or Ag were obtained on pure titanium substrate (cp-Ti, grade 2). The cp-Ti samples were sliced from a titanium bar with a diameter of 20 mm purchased from BibusMetals, AG (Essen, Germany) under the form of discs with a thickness of 2 mm.

The cp-Ti samples were ground on a SiC metallographic paper of different grits, from 320 to 800. After the grinding process, the samples were rinsed with ultrapure water, degreased using isopropyl alcohol, and cleaned in acetone for 30 min in an ultrasonic bath (Bandelin, Berlin, Germany). Subsequently they were rinsed with ultrapure water (ASTM I) and dried in air.

The electrochemical deposition was carried out in a standard electrochemical cell configured with three electrodes: working electrode (WE), reference electrode (RE), and auxiliary electrode (AE). The reference electrode was a saturated calomel electrode (SCE), while the auxiliary electrode was a platinum plate. The prepared cp-Ti discs were mounted in a Teflon samples holder, with an exposed area to the electrolyte of $\sim 2 \text{ cm}^2$. Figure 1 shows the electrochemical cell configuration used during the electrochemical experiments of undoped and doped HAp coatings deposited on cp-Ti substrate. The electrochemical deposition was performed with a potentiostat/galvanostat PARSTAT MC equipped with PMC-1000 module (Princeton Applied Research-AMETEK, Berwyn, PA, USA).

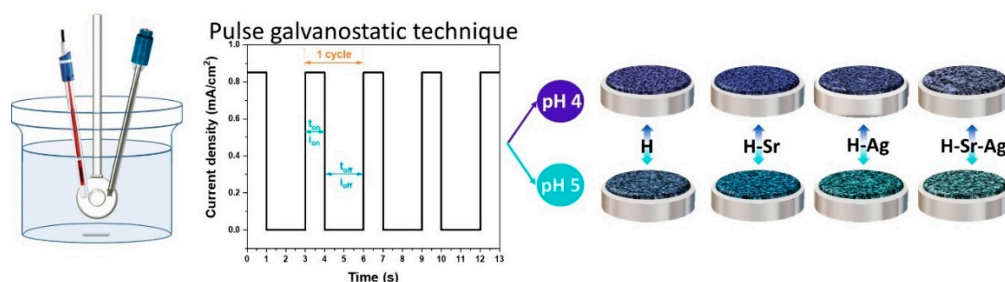


Figure 1. Electrochemical cell configuration and samples codifications.

The chemical composition of the electrolyte is shown in Table 1. The electrolyte was prepared by successive addition of reagents $\text{Ca}(\text{NO}_3)_2 \cdot 4\text{H}_2\text{O}$, $\text{NH}_4\text{H}_2\text{PO}_4$, AgNO_3 , $\text{Sr}(\text{NO}_3)_2$ in ultra-pure water (ASTM I). The reagents were purchased from Sigma Aldrich (St. Louis, MO, USA), and were of analytical grade. All electrolytes were prepared with respect to the Ca/P ratio of 1.67 [35,36].

During the electrochemically assisted deposition of HAp coatings, the electrolyte was maintained at a constant temperature of $75 \pm 0.5^\circ \text{C}$ using a magnetic stirrer/RCT with heater (IKA, Staufen im Breisgau, Germany). The deposition temperature of 75°C was selected because it favors the electrochemical deposition of crystalline HAp with enhanced features [40]. Moreover, for homogenization of the electrolyte, the solution was constantly stirred during deposition.

Table 1. Salt concentrations and element concentration ratios of the used electrolytes.

Substrate		cp-Ti			
Codifications		H	H-Sr	H-Ag	H-Sr-Ag
Chemical compositions (mM)	Ca(NO ₃) ₂ ·4H ₂ O	10	9	9.98	8.98
	NH ₄ H ₂ PO ₄			6	
	Sr(NO ₃) ₂	–	1	–	1
	AgNO ₃	–	–	0.02	0.02
(Ca + M)/P, where (M = Sr/Ag)		1.67			
pH		4 (adjusted with 1 M HNO ₃)			
		5 (adjusted with 1 M NaOH)			

The pulsed galvanostatic deposition technique was applied according to the following design: $i_{ON} = -0.85 \text{ mA/cm}^2$ was applied for 1 s, followed by a break ($i_{OFF} = 0 \text{ mA/cm}^2$) for 2 s. This cycle was repeated for 900 times, and thus the entire deposition process took 45 min. After the electrochemical depositions of the undoped and doped HAp coatings, the samples were rinsed with distilled water and dried in a hot air jet.

The current density was selected based on previous reports [28,41–43] and was selected because at low current density HAp crystals exhibit a retardant precipitation rate near the cathode, and thus the crystal grows steadily, showing a greater crystal texture [44]. Nevertheless, all the other electrochemical parameters involved in the deposition process must also be taken into consideration when developing coatings with tunable properties.

2.2. Characterization

The morphology and elemental composition for the undoped and doped hydroxyapatite coating were analyzed using a scanning electron microscope (SEM) equipped with an X-ray energy dispersive spectrometer (EDS), Phenom ProX, (Phenom World, Eindhoven, The Netherlands).

The phase composition was investigated by X-ray diffraction, using a SmartLab X-Ray (Rigaku, Tokyo, Japan) diffractometer with CuK α radiation ($\lambda = 1.5406 \text{ \AA}$) in the range $\theta/2\theta$ of 20° – 80° at an incident angle of 3° . For this purpose, a medium resolution parallel beam optical system was used. The crystallite size was calculated using the Debye-Scherrer mathematical relation (Equation (1)) for the plane (002), being the most intense diffraction peak of electrochemically obtained HAp coatings [45], while the structural properties of the samples under study were obtained from XRD diffractograms.

$$L_{(002)} = \frac{K \times \lambda}{\beta \times \cos\theta_{(002)}} \quad (1)$$

where $K = 0.9$ is a constant shape factor for HAp with hexagonal structure, β is the full width at half maximum (FWHM) measured in radian of (002) diffraction plane, and θ in degrees, indicates the Bragg's diffraction angle, $\lambda = 1.5406 \text{ \AA}$, is the wavelength of CuK α radiation.

The crystallinity (χ_c) was calculated using the following equation (Equation (2)) [46–48]:

$$\chi_c = \left(\frac{K_A}{\beta} \right)^3 \quad (2)$$

The lattice parameters of hydroxyapatite-based coatings were computed using Equation (3), the relation between the interplanar spacing distance (d_{hkl}) and lattice constants (a and c) for hexagonal crystallographic system [49,50] is as following:

$$\frac{1}{d_{hkl}^2} = \frac{4(h^2 + k^2 + l^2)}{3a^2} + \frac{1}{c^2} \quad (3)$$

The roughness of the coatings was investigated using a Dektak 150 (Veeco Instruments, Plainview, NY, USA) contact profilometer over a length of 3 mm for 60 s. From the profiles obtained were determined parameters R_a (the arithmetic average of the absolute deviations of the roughness profile from the mean value), R_q (the square root of the arithmetic mean of the squares of the deviations profile from the mean value), and R_{Sk} (factor asymmetry of the evaluated profile). For each sample a number of 10 measurements were performed and the average along with the obtained standard deviation was considered.

3. Results and Discussions

3.1. Morphology

Figure 2 shows the macroscopic appearance along with the SEM images at different magnifications of the obtained coatings for both pH values, of 4 and 5, respectively. Based on macroscopic images of the coatings after deposition, it can be observed that all coatings are fully covering the surface of the cp-Ti metallic substrate, and no defects were visible to the naked eye. Thus, from this point of view, it can be stated that the coatings were successfully achieved with respect to the selected electrochemical deposition parameters employed in this study.

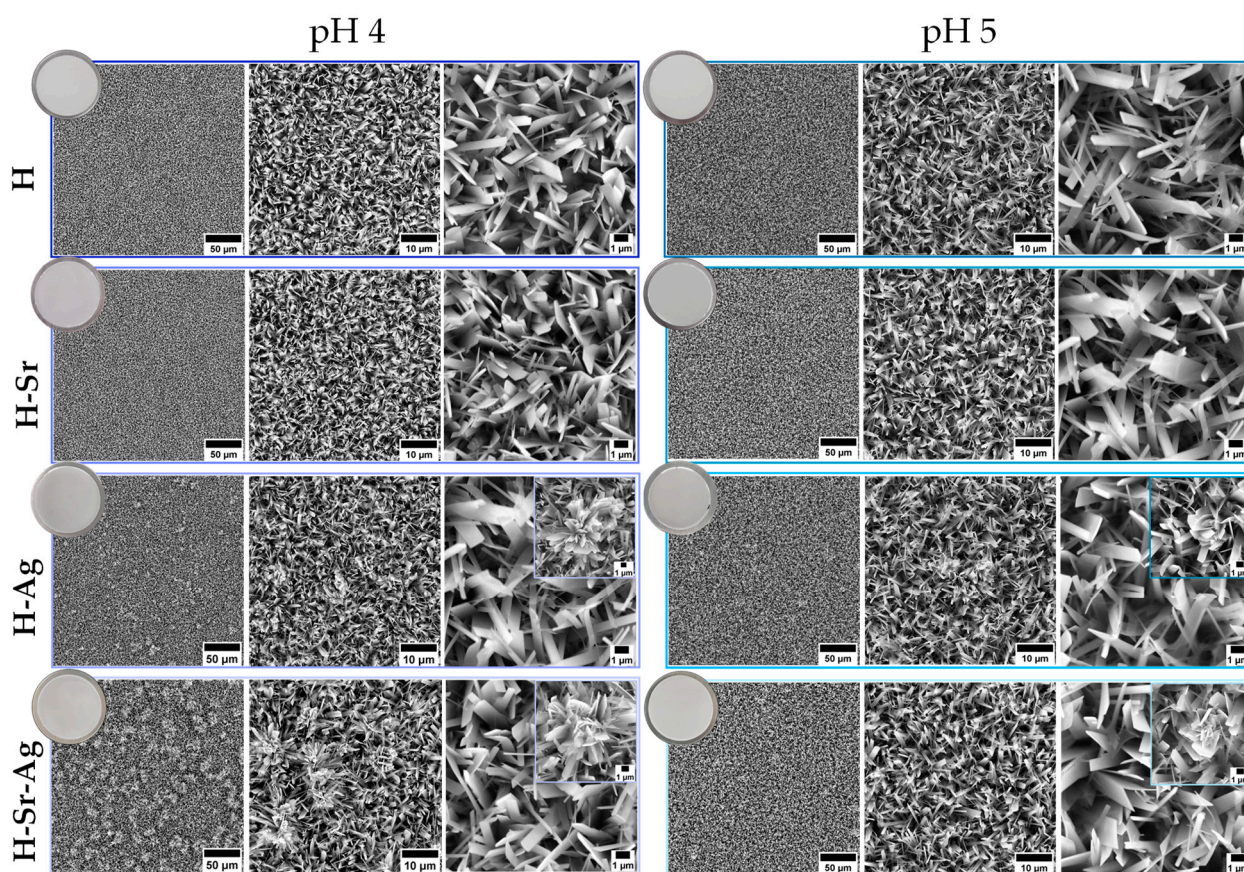


Figure 2. SEM images of hydroxyapatite-based coatings, and macroscopic images of samples after deposition (round shape).

SEM images are presented in Figure 2 and highlight that the coatings morphology consists of long and wide ribbon-like crystals with a thin in nanometric level range, regardless of the electrolyte's pH value. A possible explanation of this morphology could be attributed to electrolyte concentration [51]. The preferential direction in the crystallization process is perpendicular to the surface of the substrate along the c -axis, which corresponds to the (002) reflection, this being characteristic for the coatings obtained via electrochemical techniques [43,52].

At higher magnification, it can be noticed that the electrolyte's pH induces slight changes in terms of ribbons size, highlighting that at pH 5 the ribbons are slightly narrower. Since the dimension of the ribbon-like crystals could not be measured due to their three-dimensional orientation, only a qualitative observation could be made. Therefore, the difference between the coatings obtained at the two pH's can be represented by the crystal's density reported to the investigated area. Based on this, it can be highlighted that at more acidic pH (pH 4) the HAp crystals appear to be smaller and denser, while at higher pH (pH 5) the crystals present some increment of the crystals, forming a more uniform layer, which seems to have lower density. Thus, it can be said that by using a higher pH value, a more uniform layer consisting of crystals with similar dimensions can be obtained.

From the point of view of the doping elements added in the electrolyte, the following were observed. Even though at smaller magnification, the addition of Sr did not induce significant changes on the HAp morphology, at higher one it was observed that the crystals are narrower compared to undoped HAp coatings.

In the case of HAp doped with Ag, the predominant morphology consists in ribbons, coupled with flower-like agglomerations. These findings are consistent with the ones found in the literature [53], being usually met in electrochemical methods.

In the coatings in which both doping elements were added (H-Sr-Ag), the morphology consists of ribbons and flower-like crystals. Moreover, it was also noted that at the pH 5, the number of flowers-like agglomeration significantly decreases, emphasizing that these modifications are in strong correlation with the electrolyte's pH value.

It is widely recognized that the electrochemically synthesized hydroxyapatite can nucleate and grow under various morphologies which sensitively depend on the specific growth conditions [54,55]. In galvanostatic technique, higher reaction rates for phosphate and hydroxyl ion are enforced, influencing the chemical precipitation reaction and thus, the layer morphology and growth rates [56]. Of course, the electrolytes should not be neglected, since a more acidic pH leads to the formation of a higher quantity of hydrogen gas and thus the reactions are more energetic [31]. Nevertheless, because the coatings are deposited in pulses, the repeatedly interrupted process of nucleation and growth of precipitates at, theoretically, nearly constant ion concentrations lead to structures that are usually more compact and uniform.

3.2. Elemental Composition

The EDS analysis (Table 2) revealed the presence of Ti from cp-Ti used as substrate, but also the elements characteristic for hydroxyapatite (Ca, P, and O) as well as the doping elements (Ag and Sr), indicating that the coatings were successfully achieved by pulse galvanostatic technique.

Table 2. Chemical composition of the coatings at different pH values.

pH	Sample	Chemical Composition (at.%)				(Ca + M)/P (Where, M = Sr, Ag, Sr + Ag)
		Ca	P	Sr	Ag	
4	H	60.70	39.30	–	–	1.54
	H-Sr	55.62	40.85	3.52	–	1.45
	H-Ag	60.17	38.16	–	1.67	1.62
	H-Sr-Ag	54.88	39.89	3.43	1.80	1.51
5	H	61.18	38.82	–	–	1.58
	H-Sr	56.38	40.16	3.45	–	1.49
	H-Ag	61.14	37.82	–	1.04	1.64
	H-Sr-Ag	56.39	39.41	3.34	0.86	1.54

Because both elements Ag and Sr ions substitute the Ca ions found in the HAp lattice, the (Ca + M)/P ratio was calculated [43,57–59], where M is the doping element, Sr, or/and Ag, respectively. In Table 2 is presented the chemical composition of all the coatings obtained at different pH values. In terms of Ca/P ratio evolution, the obtained coatings registered a ratio below the stoichiometric one of 1.67, indicating that all coatings are

Ca-deficient, which according to some studies may be beneficial, since calcium phosphate's constitution in human bones is non-stoichiometric [60–62].

By comparing the same coating type at the two pH's selected, it can be observed that a higher pH leads to an enhancement of the Ca/P ratios (Figure 3a), with values closer to the stoichiometric one. In terms of doping element, it can be observed that irrespective of the pH value (Figure 3a), the H-Ag coatings have registered the highest Ca/P ratio, of 1.62 at pH 4 and 1.64 at pH 5, while the lowest were obtained for the H-Sr coatings, of 1.45 at pH 4 and 1.49 at pH 5. By co-doping the HAp with Sr and Ag, the obtained ratios were found to be between the highest and lowest values, with values of 1.51 at pH 4 and 1.54 at pH 5. Overall, it can be said that the addition of Ag increases the Ca/P ratio, Sr decreases it, while when both elements are added, it can be observed that the two elements are competing each other, leading to a ratio that is slightly higher than the one obtained for the H-Sr coatings, indicating that the addition of Ag in the H-Sr coatings has a beneficial effect.

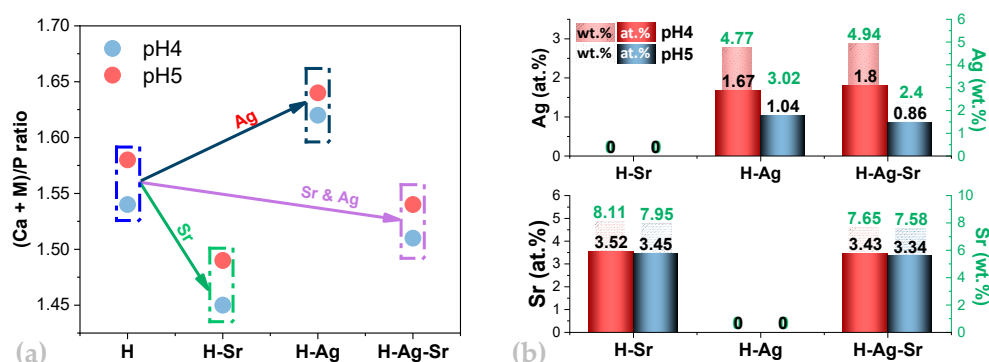


Figure 3. Evolution of (Ca + M)/P ratio (a) and doping element concentration (Ag, Sr and Ag & Sr) in each coating expressed in at.% and wt.% (b).

Another important aspect highlighted by the EDS analysis was that by increasing the pH value from 4 to 5, the at.% of Ag was reduced from 1.80 to 0.86 in the co-doped coatings (H-Sr-Ag), and from 1.67 to 1.08 for the H-Ag coatings, indicating that even though the initial silver concentration is the same, the pH value strongly influences the Ag content in the HAp-based coatings (Figure 3b). A similar observation was also made by Narendran et al. [63], which has evidenced that by increasing the pH value, the Ag amount decreases. Oppositely, the Sr quantity remains approximately at the same values (between 3.40 at.% and 3.52 at.%), irrespective of the pH level or the coating type (H-Sr and/or H-Sr-Ag).

The silver quantity and its chemical stability within the material is of crucial importance since a quantity of 6 wt.% of Ag [64], can induce not just the desired antibacterial effect but also cell apoptosis, which in medical applications must be avoided or, if not possible, at least to be reduced at minimum. In accordance with the in vitro assays on human osteoblasts, an Ag content between 2 wt.% and 4 wt.% provides a fine balance between cytotoxicity and antimicrobial activity [64,65]. Within this context, it must be said that the H-Ag and H-Sr-Ag coatings at pH 5 had values lower than 4 wt.%, of 3.02 wt.%, and 2.40 wt.%, respectively, while at pH 4 both coatings had values of ~4.8 wt.% (Figure 3b).

In a study performed by Ciuca et al. [17] it was proven that 2 at.% of Ag is sufficient to enhance the resistance to *candida albicans*, a Gram-positive bacteria, known to affect prosthetic joints [66–68], while Badea et al. [20] highlighted that even a small quantity of Ag (0.7 at.%) into hydroxyapatite coatings can improve the antibacterial properties of hydroxyapatite.

Since the amount of Ag is of critical importance, a balance between these two characteristics, antibacterial effect, and biocompatibility [59], must be taken into consideration when designing a material. Thus, based on these findings, it can be stated that by using a pH of 5, the Ag amount can be obtained within its optimum concentration in terms of antibacterial effect without affecting the cell behavior.

3.3. Phase Composition

The XRD diffractograms of the undoped and doped HAp presented in Figure 4, revealed that all obtained coatings consist of hydroxyapatite (HAp, card no. 09-0432) as the main phase in accordance with the International Center for Diffraction Data (ICDD), regardless the pH of the electrolyte.

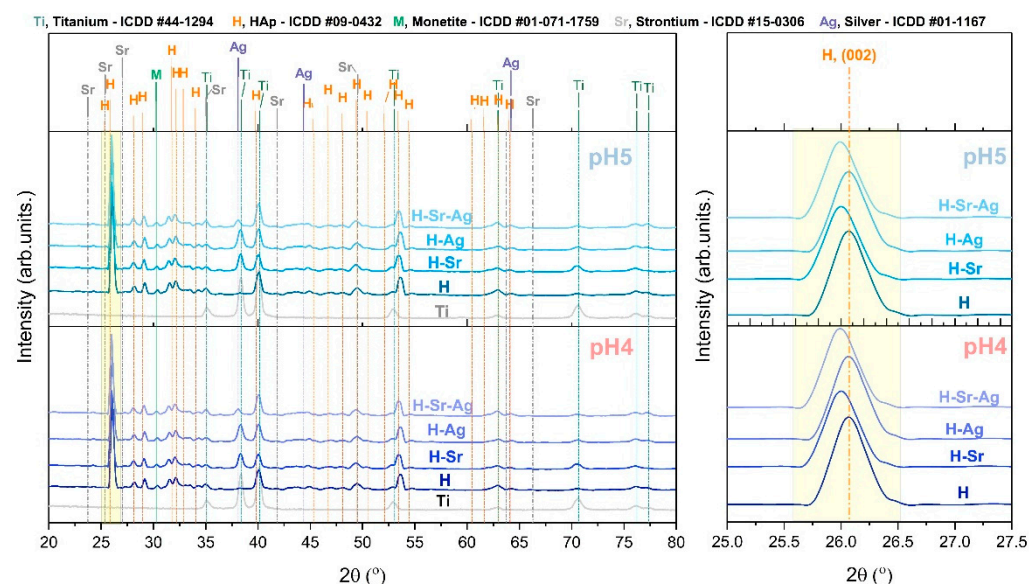


Figure 4. XRD diffractograms of the electrochemically deposited coatings on Ti substrate.

A small diffraction peak located at 30.31° was assigned to monetite (CaHPO_4) according to ICDD card No. 01-071-1759, indicating the presence of a secondary phase. Monetite is an important calcium phosphate precursor that promotes cell proliferation, being recognized for its osseointegrative and osteoconductive character [69].

Even though, the XRD analysis was performed in grazing mode, the XRD diffractograms also showed the diffraction peaks specific to the titanium substrate according to ICDD card No. 044-1298, and indirectly suggesting that the coatings are not very thick.

With respect to the main phase of the coatings, attributed to HAp, the maximum diffraction intensity found at 2θ of $\sim 26^\circ$ indicates that the preferential orientation is in the direction of the c -axis, according to (002) plan, which is in good agreement with the SEM images, in which was shown that the HAp crystals grow perpendicular on the substrate surface. These findings are similar to the ones already reported in the literature [70–72] and which have proven that crystalline HAp with a c -axis orientation increases the capacity of osseointegration, by promoting cell proliferation, and presenting a higher chemical stability.

No specific peaks of Ag and/or Sr in metallic form were identified by XRD analysis.

Due to the differences among the ionic radius of Ca^{2+} (0.99 Å), Sr^{2+} (1.2 Å), and Ag^+ (1.28 Å), the diffraction peaks shifted toward smaller angles (Figure 4) with the addition of Sr^{2+} and Ag^+ denoting an expansion in the crystal lattice caused by the partial incorporation of Ag and/or Sr into HAp, rather than just a surface modification [23,73].

In Table 3 is presented the degree of crystallinity, lattice parameters, and crystallite sizes.

A narrower peak suggests that both lattice parameters and the crystallinity increase [74]. Thus, compared to HAp, addition of the doping elements with higher ionic radius than Ca has led to an increment of the lattice parameters a and c , which is in good agreement with other studies [75–77]. However, by increasing the electrolyte's pH to 5, the lattice parameters presented slightly higher values for the same coating type. The same trend was also noted for the crystallinity degree which had values between 46% and 50%, but also

for the crystallite dimension, indicating that a higher pH value favors the development of more crystalline HAp-based coatings.

Table 3. Lattice parameters, crystallite dimension, and crystallinity calculated for the HAp-based coatings.

<div>Parameters</div> <div>pH and Sample</div>		2θ (°) for (002) Reflection	Crystallite Size L ₍₀₀₂₎ (nm)	Lattice Constants		Crystallinity (%)
				a = b (Å)	c (Å)	
H (#09-0432)		25.88	N/A	9.418	6.884	N/A
pH 4	H	26.09	26.04	9.418	6.861	46.55
	H-Sr	26.08	26.39	9.442	6.883	48.46
	H-Ag	26.03	26.65	9.423	6.872	49.93
	H-Sr-Ag	26	26.47	9.444	6.89	48.91
pH 5	H	26.07	26.11	9.423	6.865	46.92
	H-Sr	26.05	26.4	9.446	6.876	48.52
	H-Ag	26.01	26.31	9.426	6.867	48.05
	H-Sr-Ag	25.99	26.57	9.445	6.888	49.49

It can be observed that the H-Sr coatings, irrespective of pH value, present very close crystallite dimension and crystallinity. By correlating these results (Figure 5) with EDS analysis, which highlighted that Sr is found in approximately equal amounts (3.52 at.% at pH 4 and 3.45 at.% at pH 5), it can be stated that the electrolyte's pH does not have such a great effect on the quantities of Sr as dopant in HAp structure, nor the crystallite dimension or crystallinity.

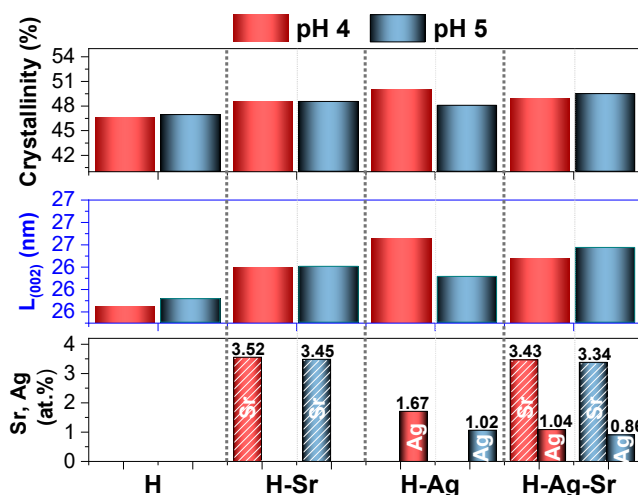


Figure 5. Correlation between crystallite dimension, crystallinity and at.% of Sr and/or Ag in the coatings.

Oppositely, Ag appears to be dependent on the pH value, revealing a different behavior. Thus, at higher pH, the crystallite dimension and crystallinity decrease, which was to be expected since a smaller quantity of Ag (1.02 at.%) was observed in H-Ag coatings at pH 5.

By co-doping the HAp coatings with Ag and Sr (H-Sr-Ag), the crystallite dimension and crystallinity have registered an increment at pH 5, compared to pH 4. These results can also be correlated with the elemental composition but also with the competition between Sr and Ag.

Thus, as a general observation, it can be said that XRD analysis has confirmed that the HAp-based coatings are doped with Ag and/or Sr and that by increasing the pH value from 4 to 5, the crystallinity degree increases.

3.4. Roughness

Beside phase composition, and crystallinity of the coatings, surface free energy, porosity, as well as their surface roughness play important parts in the pursuit for enhancing the biomedical performance of implantable materials [6]. Surface roughness is among the characteristics that can affect the cell behavior [78]. Thus, osteoblasts prefer a rougher surface, while fibroblasts prefer a smoother surface [79]. Usually, it is classified into macro and nano-roughness, and each of them influences the properties of the surface differently [80]. Regarding the effect of the roughness on the bacteria attachment, it should be said that this is a very complex process which is controlled by interplay between physico-chemical, topographical surface properties, bacterial characteristics, and environmental conditions [81]. Thus, a correlation between bacterial adhesion and just the surface roughness is challenging or even impossible to make, since more aspects need to be taken into consideration.

In Figures 6 and 7 are presented the profile lines specific for each coating and the main roughness parameters.

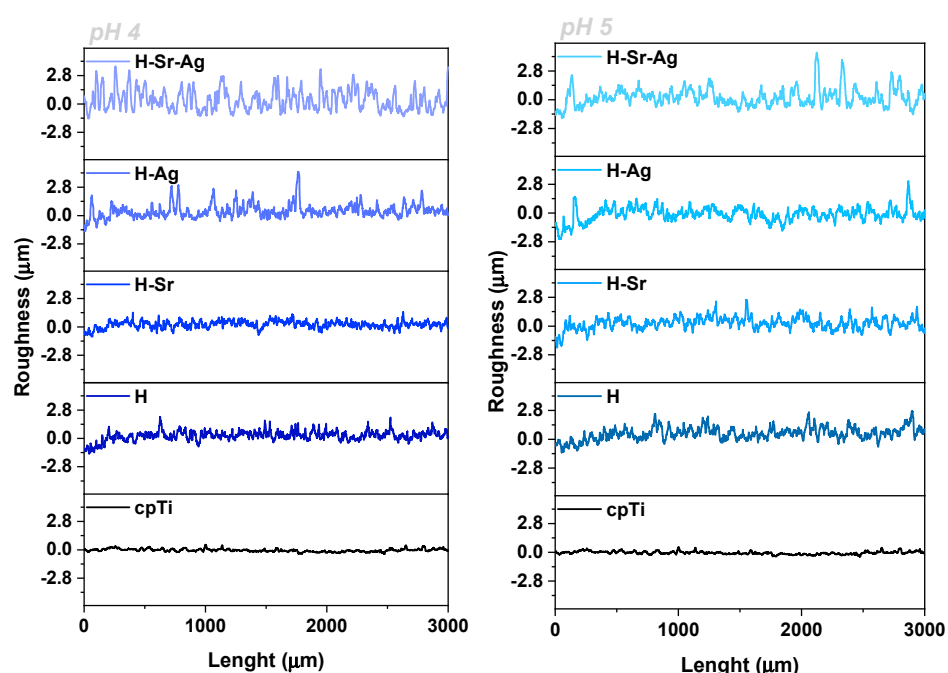


Figure 6. Roughness profiles of the investigated coatings at pH 4 (left) and pH 5 (right).

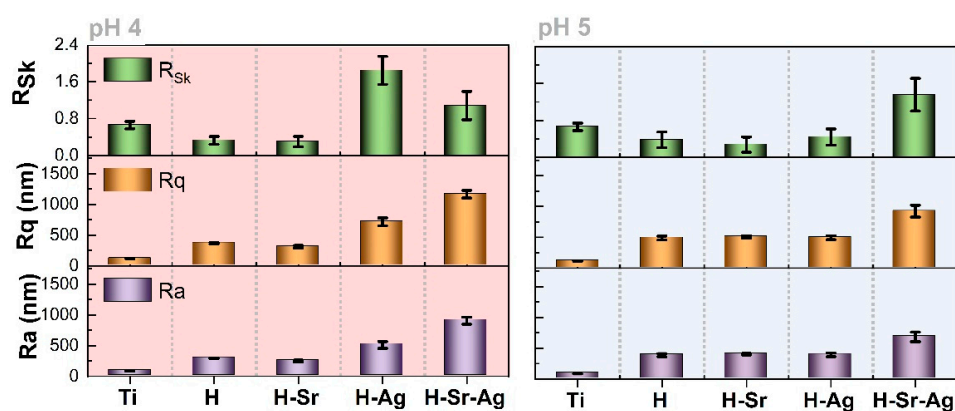


Figure 7. Roughness parameters of the HAp-based coatings and substrate at pH 4 (left) and pH 5 (right).

According to the obtained results, it can be stated that by increasing the pH value from 4 to 5, the average roughness (Ra) and root mean square roughness (Rq) parameters present some modifications with respect to the doping elements and pH value as following.

As a general remark, all coatings have registered higher R_a than the Ti substrate ($R_a = 86$ nm). By comparing the undoped HAp at the two selected pHs, it can be observed that by increasing the pH level, the R_a parameter also increased with ~ 100 nm. A similar trend is also visible for the coatings doped with Sr, which at pH 5 had an R_a of 403 nm, compared to 248 nm obtained at pH 4. Addition of Ag in the H-Ag or H-Sr-Ag coatings has led to a decrement of the roughness at higher pH value, from 510 and 904 to values of 390 and 684 nm, respectively. These findings can be correlated with the SEM images, which have highlighted that compared to pH 5, at lower pH value, multiple flower-like formations were found. Thus, the presence of these morphologies, can explain the higher roughness obtained at pH 4 for the H-Ag and H-Sr-Ag coatings.

The asymmetry of the surface distribution also known as skewness (R_{Sk}) provides information on the distribution of hills (slope < 0) for an area with deeper valleys, and the distribution of the valleys (slope > 0) for an area with higher hills. Thus, based on this criterion, all the coatings showed a positive asymmetry, suggesting that all surfaces are predominant in hills. Nevertheless, just as observed for R_a parameter, the addition of Ag at lower pH values, generated higher hills compared to the ones obtained at higher pH, and thus a higher R_{Sk} , most likely due to the presence of the flower-like crystals.

Moreover, by comparing the R_{Sk} parameter of the Ti substrate, with the ones obtained for the coatings, a decrement can be observed indicating that the coatings tend to smoothen the surface. It was also noted that the coatings obtained at pH 5 present a lower R_{Sk} than the ones obtained at pH 4.

In a study performed by Evgeny et al. [82] it was found that increasing positive skewness is an advantage for having good corrosion resistance, while surfaces with negative skewness mainly exhibit pitting corrosion. The surface with negative skewness consists in many grooves which could develop the micro- reaction sites and trap the corrosion products formed at the base of the grooves, which can accelerate the growth of pits. Skewness parameter can also be correlated with other types of investigations such as biodegradation because changes of this parameter could be used to monitor time-dependent biodegradation of materials [83].

Thus, by increasing the pH level, a more uniform surface with an average roughness between 380 and 680 nm, and a tendency toward a symmetrical topography, can be obtained, irrespective of the doping element used.

4. Conclusions

According to this study, the galvanostatic pulse technique is a versatile technique that allows to obtain uniform coatings and the pH of the electrolyte is among the most important parameters involved in the deposition process. Thus, at a higher pH, more uniform layers were obtained, regardless of the doping element, with a Ca/P ratio closer to the stoichiometric hydroxyapatite and higher crystallinity. The doping elements were successfully substituted in the HAp structure regardless the electrolyte's pH, this aspect being highlighted by XRD analysis, which have also shown that addition of elements with a higher ionic radius than Ca, lead to an increment of the lattice parameters. The crystallite dimension has increased with respect to the doping elements added. Moreover, irrespective of the doping element used, it was shown that the HAp coatings obtained at a pH of 5 present a more uniform surface with an average roughness between 380 and 680 nm, and a tendency toward a symmetrical topography.

Nevertheless, the present study has also highlighted one important aspect, namely that the pH value of the electrolytes has a weak influence on the quantities of Sr as dopant, while Ag is in strong dependency with the pH value at which the electrochemical deposition is carried out, as demonstrated by the SEM, EDS, and XRD analysis.

Within the limitations of the current study, it can be said that the coatings obtained at pH 5 revealed superior properties compared to those obtained at pH 4, and addition of Ag and Sr also play important parts in developing such type of coatings. Nevertheless, the mechanism governing such an enhancement is not clearly understood and further

studies must be made. Thus, as future direction, the coatings obtained at higher pH will be further evaluated in terms of electrochemical behavior in synthetic media, along with their biomineralization ability and in vitro cells behavior.

Author Contributions: Conceptualization, D.M.V. and E.U.; methodology, C.M.C.; validation, A.V. and M.T.; investigation, E.U., A.C.P. and D.M.V.; data curation, C.M.C. and A.V.; writing—original draft preparation, E.U. and D.M.V.; writing—review and editing, C.M.C., D.M.V. and A.V.; visualization, E.U. and D.M.V. All authors have read and agreed to the published version of the manuscript.

Funding: This work was supported by a grant of the Romanian Ministry of Education and Research, CNCS—UEFISCDI, project number PN-III-P1-1.1-TE-2019-1331, within PNCDI III (Grant No. TE 172/2020; 3B-CoatED).

Institutional Review Board Statement: Not applicable.

Informed Consent Statement: Not applicable.

Data Availability Statement: Data sharing is not applicable to this article.

Acknowledgments: A.V. thanks to Tomsk Polytechnic University within the framework of the Tomsk Polytechnic University—Competitiveness Enhancement Program grant. This work was supported by a grant of the Romanian National Authority for Scientific Research and Innovation CCCDI-UEFISCDI, project COFUND-ERANET EURONANOMED 3-NANO-VERTEBRA, within PNCDI III (Grant No. 91/2019) as well as the Core Program of 2019 (Grant No. 18N/2019).

Conflicts of Interest: The authors declare no conflict of interest.

References

1. Prasad, K.; Bazaka, O.; Chua, M.; Rochford, M.; Fedrick, L.; Spoor, J.; Symes, R.; Tieppo, M.; Collins, C.; Cao, A.; et al. Metallic Biomaterials: Current Challenges and Opportunities. *Materials* **2017**, *10*, 884. [\[CrossRef\]](#)
2. Abdel-Hady Gepreel, M.; Niinomi, M. Biocompatibility of Ti-Alloys for Long-Term Implantation. *J. Mech. Behav. Biomed. Mater.* **2013**, *20*, 407–415. [\[CrossRef\]](#) [\[PubMed\]](#)
3. Cotrut, C.; Parau, A.; Gherghilescu, A.; Titorencu, I.; Pana, I.; Cojocaru, D.; Pruna, V.; Constantin, L.; Dan, I.; Vranceanu, D.; et al. Mechanical, In Vitro Corrosion Resistance and Biological Compatibility of Cast and Annealed Ti25Nb10Zr Alloy. *Metals* **2017**, *7*, 86. [\[CrossRef\]](#)
4. Kaur, M.; Singh, K. Review on Titanium and Titanium Based Alloys as Biomaterials for Orthopaedic Applications. *Mater. Sci. Eng. C* **2019**, *102*, 844–862. [\[CrossRef\]](#) [\[PubMed\]](#)
5. Beig, B.; Liaqat, U.; Niazi, M.F.K.; Douna, I.; Zahoor, M.; Niazi, M.B.K. Current Challenges and Innovative Developments in Hydroxyapatite-Based Coatings on Metallic Materials for Bone Implantation: A Review. *Coatings* **2020**, *10*, 1249. [\[CrossRef\]](#)
6. Safavi, M.S.; Walsh, F.C.; Surmeneva, M.A.; Surmenev, R.A.; Khalil-Allafi, J. Electrodeposited Hydroxyapatite-Based Biocoatings: Recent Progress and Future Challenges. *Coatings* **2021**, *11*, 110. [\[CrossRef\]](#)
7. Graziani, G.; Boi, M.; Bianchi, M. A Review on Ionic Substitutions in Hydroxyapatite Thin Films: Towards Complete Biomimeticism. *Coatings* **2018**, *8*, 269. [\[CrossRef\]](#)
8. Ressler, A.; Žužić, A.; Ivanišević, I.; Kamboj, N.; Ivanković, H. Ionic Substituted Hydroxyapatite for Bone Regeneration Applications: A Review. *Open Ceramics* **2021**, *6*, 100122. [\[CrossRef\]](#)
9. Jiang, Y.; Yuan, Z.; Huang, J. Substituted Hydroxyapatite: A Recent Development. *Mater. Technol.* **2020**, *35*, 785–796. [\[CrossRef\]](#)
10. Querido, W.; Rossi, A.L.; Farina, M. The Effects of Strontium on Bone Mineral: A Review on Current Knowledge and Microanalytical Approaches. *Micron* **2016**, *80*, 122–134. [\[CrossRef\]](#)
11. Marie, P.J.; Ammann, P.; Boivin, G.; Rey, C. Mechanisms of Action and Therapeutic Potential of Strontium in Bone. *Calcif. Tissue Int.* **2001**, *69*, 121. [\[CrossRef\]](#) [\[PubMed\]](#)
12. Kazemi, M.; Dehghan, M.M.; Azami, M. Biological Evaluation of Porous Nanocomposite Scaffolds Based on Strontium Substituted β -TCP and Bioactive Glass: An in Vitro and in Vivo Study. *Mater. Sci. Eng. C* **2019**, *105*, 110071. [\[CrossRef\]](#) [\[PubMed\]](#)
13. Marx, D.; Rahimnejad Yazdi, A.; Papini, M.; Towler, M. A Review of the Latest Insights into the Mechanism of Action of Strontium in Bone. *Bone Rep.* **2020**, *12*, 100273. [\[CrossRef\]](#)
14. Tran, T.T.; Nichita, N.B.; Dobrica, M.O.; Cotrut, C.M.; Vranceanu, M.D.; Tarcolea, M. In Vitro Biocompatibility Investigation of Silver and Zinc Modified Hydroxyapatite Deposited on Implant Materials. *UPB Sci. Bull. Ser. B Chem. Mater. Sci.* **2020**, *82*, 231–245.
15. Vranceanu, D.M.; Parau, A.C.; Cotrut, C.M.; Kiss, A.E.; Constantin, L.R.; Braic, V.; Vladescu, A. In Vitro Evaluation of Ag Doped Hydroxyapatite Coatings in Acellular Media. *Ceram. Int.* **2019**, *45*, 11050–11061. [\[CrossRef\]](#)
16. Ciobanu, C.S.; Iconaru, S.L.; Pasuk, I.; Vasile, B.S.; Lupu, A.R.; Hermenean, A.; Dinischiotu, A.; Predoi, D. Structural Properties of Silver Doped Hydroxyapatite and Their Biocompatibility. *Mater. Sci. Eng. C* **2013**, *33*, 1395–1402. [\[CrossRef\]](#)

17. Ciuca, S.; Badea, M.; Pozna, E.; Pana, I.; Kiss, A.; Floroian, L.; Semenescu, A.; Cotrut, C.M.; Moga, M.; Vladescu, A. Evaluation of Ag Containing Hydroxyapatite Coatings to the Candida Albicans Infection. *J. Microbiol. Methods* **2016**, *125*, 12–18. [[CrossRef](#)] [[PubMed](#)]
18. Chen, Y.; Zheng, X.; Xie, Y.; Ding, C.; Ruan, H.; Fan, C. Anti-Bacterial and Cytotoxic Properties of Plasma Sprayed Silver-Containing HA Coatings. *J. Mater. Sci. Mater. Med.* **2008**, *19*, 3603–3609. [[CrossRef](#)]
19. Sandukas, S.; Yamamoto, A.; Rabiei, A. Osteoblast Adhesion to Functionally Graded Hydroxyapatite Coatings Doped with Silver. *J. Biomed. Mater. Res. Part A* **2011**, *97*, 490–497. [[CrossRef](#)]
20. Badea, M.; Braic, M.; Kiss, A.; Moga, M.; Pozna, E.; Pana, I.; Vladescu, A. Influence of Ag Content on the Antibacterial Properties of SiC Doped Hydroxyapatite Coatings. *Ceram. Int.* **2016**, *42*, 1801–1811. [[CrossRef](#)]
21. Geng, Z.; Cui, Z.; Li, Z.; Zhu, S.; Liang, Y.; Liu, Y.; Li, X.; He, X.; Yu, X.; Wang, R.; et al. Strontium Incorporation to Optimize the Antibacterial and Biological Characteristics of Silver-Substituted Hydroxyapatite Coating. *Mater. Sci. Eng. C* **2016**, *58*, 467–477. [[CrossRef](#)]
22. Geng, Z.; Wang, R.; Zhuo, X.; Li, Z.; Huang, Y.; Ma, L.; Cui, Z.; Zhu, S.; Liang, Y.; Liu, Y.; et al. Incorporation of Silver and Strontium in Hydroxyapatite Coating on Titanium Surface for Enhanced Antibacterial and Biological Properties. *Mater. Sci. Eng. C* **2017**, *71*, 852–861. [[CrossRef](#)] [[PubMed](#)]
23. Huang, Y.; Zhang, X.; Zhang, H.; Qiao, H.; Zhang, X.; Jia, T.; Han, S.; Gao, Y.; Xiao, H.; Yang, H. Fabrication of Silver- and Strontium-Doped Hydroxyapatite/TiO₂ Nanotube Bilayer Coatings for Enhancing Bactericidal Effect and Osteoinductivity. *Ceram. Int.* **2017**, *43*, 992–1007. [[CrossRef](#)]
24. Dhinasekaran, D.; Kaliaraj, G.S.; Jagannathan, M.; Rajendran, A.R.; Prakasarao, A.; Ganesan, S.; Subramanian, B. Pulsed Laser Deposition of Nanostructured Bioactive Glass and Hydroxyapatite Coatings: Microstructural and Electrochemical Characterization. *Mater. Sci. Eng. C* **2021**, *130*, 112459. [[CrossRef](#)]
25. Chambard, M.; Marsan, O.; Charvillat, C.; Grossin, D.; Fort, P.; Rey, C.; Gitzhofer, F.; Bertrand, G. Effect of the Deposition Route on the Microstructure of Plasma-Sprayed Hydroxyapatite Coatings. *Surf. Coat. Technol.* **2019**, *371*, 68–77. [[CrossRef](#)]
26. Mohammad, N.F.; Ahmad, R.N.; Mohd Rosli, N.L.; Abdul Manan, M.S.; Marzuki, M.; Wahi, A. Sol Gel Deposited Hydroxyapatite-Based Coating Technique on Porous Titanium Niobium for Biomedical Applications: A Mini Review. *Mater. Today Proc.* **2020**, *41*, 127–135. [[CrossRef](#)]
27. Drevet, R.; Ben Jaber, N.; Fauré, J.; Tara, A.; Ben Cheikh Larbi, A.; Benhayoune, H. Electrophoretic Deposition (EPD) of Nano-Hydroxyapatite Coatings with Improved Mechanical Properties on Prosthetic Ti6Al4V Substrates. *Surf. Coat. Technol.* **2016**, *301*, 94–99. [[CrossRef](#)]
28. Blackwood, D.J.; Seah, K.H.W. Galvanostatic Pulse Deposition of Hydroxyapatite for Adhesion to Titanium for Biomedical Purposes. *Mater. Sci. Eng. C* **2010**, *30*, 561–565. [[CrossRef](#)]
29. Zhu, J.; Sun, H.H.; Wo, J.; Xu, F.H.; Lu, W.Q.; Deng, B.; Zhu, Y.Y.; Yuan, F. Duration of Electrochemical Deposition Affects the Morphology of Hydroxyapatite Coatings on 3D-Printed Titanium Scaffold as Well as the Functions of Adhered MC3T3-E1 Cells. *J. Orthop. Sci.* **2020**, *25*, 708–714. [[CrossRef](#)] [[PubMed](#)]
30. Uklejewski, R.; Rogala, P.; Winiecki, M.; Toklowicz, R.; Ruszkowski, P.; Woluń-Cholewa, M. Biomimetic Multispiked Connecting Ti-Alloy Scaffold Prototype for Entirely-Cementless Resurfacing Arthroplasty Endoprostheses-Exemplary Results of Implantation of the Ca-P Surface-Modified Scaffold Prototypes in Animal Model and Osteoblast Culture Evaluat. *Materials* **2016**, *9*, 532. [[CrossRef](#)]
31. Vladescu, A.; Vranceanu, D.M.; Kulesza, S.; Ivanov, A.N.; Bramowicz, M.; Fedonnikov, A.S.; Braic, M.; Norkin, I.A.; Koptuyg, A.; Kurtukova, M.O.; et al. Influence of the Electrolyte's PH on the Properties of Electrochemically Deposited Hydroxyapatite Coating on Additively Manufactured Ti64 Alloy. *Sci. Rep.* **2017**, *7*, 4–7. [[CrossRef](#)] [[PubMed](#)]
32. Thanh, D.T.M.; Nam, P.T.; Phuong, N.T.; Que, L.X.; van Anh, N.; Hoang, T.; Lam, T.D. Controlling the Electrodeposition, Morphology and Structure of Hydroxyapatite Coating on 316L Stainless Steel. *Mater. Sci. Eng. C* **2013**, *33*, 2037–2045. [[CrossRef](#)] [[PubMed](#)]
33. Hu, R.; Lin, C.; Shi, H.; Wang, H. Electrochemical Deposition Mechanism of Calcium Phosphate Coating in Dilute Ca-P Electrolyte System. *Mater. Chem. Phys.* **2009**, *115*, 718–723. [[CrossRef](#)]
34. Qiao, H.; Song, G.; Huang, Y.; Yang, H.; Han, S.; Zhang, X.; Wang, Z.; Ma, J.; Bu, X.; Fu, L. Si, Sr, Ag Co-Doped Hydroxyapatite/TiO₂ Coating: Enhancement of Its Antibacterial Activity and Osteoinductivity. *RSC Adv.* **2019**, *9*, 13348–13364. [[CrossRef](#)]
35. Eliaz, N.; Sridh, T.M. Electrocrystallization of Hydroxyapatite and Its Dependence on Solution Conditions. *Cryst. Growth Des.* **2008**, *8*, 3965–3977. [[CrossRef](#)]
36. Sun, Q.; Yang, Y.; Luo, W.; Zhao, J.; Zhou, Y. The Influence of Electrolytic Concentration on the Electrochemical Deposition of Calcium Phosphate Coating on a Direct Laser Metal Forming Surface. *Int. J. Anal. Chem.* **2017**, *2017*, 8610858. [[CrossRef](#)]
37. Djošić, M.S.; Panić, V.; Stojanović, J.; Mitrić, M.; Miskovic-Stankovic, V.B. The Effect of Applied Current Density on the Surface Morphology of Deposited Calcium Phosphate Coatings on Titanium. *Colloids Surf. A Physicochem. Eng. Asp.* **2012**, *400*, 36–43. [[CrossRef](#)]
38. Benhayoune, H.; Drevet, R.; Fauré, J.; Potiron, S.; Gloriant, T.; Oudadesse, H.; Laurent-Maquin, D. Elaboration of Monophasic and Biphasic Calcium Phosphate Coatings on Ti6Al4V Substrate by Pulsed Electrodeposition Current. *Adv. Eng. Mater.* **2010**, *12*, 192–199. [[CrossRef](#)]

39. Dumelié, N.; Benhayoune, H.; Rousse-Bertrand, C.; Bouthors, S.; Perchet, A.; Wortham, L.; Douglade, J.; Laurent-Maquin, D.; Balossier, G. Characterization of Electrodeposited Calcium Phosphate Coatings by Complementary Scanning Electron Microscopy and Scanning-Transmission Electron Microscopy Associated to X-Ray Microanalysis. *Thin Solid Film.* **2005**, *492*, 131–139. [\[CrossRef\]](#)
40. Cotrut, C.M.; Vladescu, A.; Dinu, M.; Vranceanu, D.M. Influence of Deposition Temperature on the Properties of Hydroxyapatite Obtained by Electrochemical Assisted Deposition. *Ceram. Int.* **2018**, *44*, 669–677. [\[CrossRef\]](#)
41. Huang, Y.; Zhang, X.; Qiao, H.; Hao, M.; Zhang, H.; Xu, Z. Corrosion Resistance and Cytocompatibility Studies of Zinc-Doped Fl Urohydroxyapatite Nanocomposite Coatings on Titanium Implant. *Ceram. Int.* **2016**, *42*, 1903–1915. [\[CrossRef\]](#)
42. Yan, Y.; Ding, Q.; Huang, Y.; Han, S.; Pang, X. Magnesium Substituted Hydroxyapatite Coating on Titanium with Nanotubular TiO₂ Intermediate Layer via Electrochemical Deposition. *Appl. Surf. Sci.* **2014**, *305*, 77–85. [\[CrossRef\]](#)
43. Vranceanu, D.M.; Ionescu, I.C.; Ungureanu, E.; Cojocaru, M.O.; Vladescu, A.; Cotrut, C.M. Magnesium Doped Hydroxyapatite-Based Coatings Obtained by Pulsed Galvanostatic Electrochemical Deposition with Adjustable Electrochemical Behavior. *Coatings* **2020**, *10*, 727. [\[CrossRef\]](#)
44. Li, T.-T.; Ling, L.; Lin, M.-C.; Peng, H.-K.; Ren, H.-T.; Lou, C.-W.; Lin, J.-H. Recent Advances in Multifunctional Hydroxyapatite Coating by Electrochemical Deposition. *J. Mater. Sci.* **2020**, *55*, 6352–6374. [\[CrossRef\]](#)
45. Blackwood, D.J.; Seah, K.H.W. Electrochemical Cathodic Deposition of Hydroxyapatite: Improvements in Adhesion and Crystallinity. *Mater. Sci. Eng. C* **2009**, *29*, 1233–1238. [\[CrossRef\]](#)
46. Landi, E.; Tampieri, A.; Celotti, G.; Sprio, S. Densification Behaviour and Mechanisms of Synthetic Hydroxyapatites. *J. Eur. Ceram. Soc.* **2000**, *20*, 2377–2387. [\[CrossRef\]](#)
47. Gopi, D.; Kanimozhi, K.; Bhuvaneshwari, N.; Indira, J.; Kavitha, L. Novel Banana Peel Pectin Mediated Green Route for the Synthesis of Hydroxyapatite Nanoparticles and Their Spectral Characterization. *Spectrochim. Acta Part A Mol. Biomol. Spectrosc.* **2014**, *118*, 589–597. [\[CrossRef\]](#)
48. Rusu, V.; Chuen-How, N.; Wilke, M.; Tiersch, B.; Fratzl, P.; Peter, M. Size-Controlled Hydroxyapatite Nanoparticles as Self-Organized Organic-Inorganic Composite Materials. *Biomaterials* **2005**, *26*, 5414–5426. [\[CrossRef\]](#) [\[PubMed\]](#)
49. Li, Z.Y.; Lam, W.M.; Yang, C.; Xu, B.; Ni, G.X.; Abbah, S.A.; Cheung, K.M.C.; Luk, K.D.K.; Lu, W.W. Chemical Composition, Crystal Size and Lattice Structural Changes after Incorporation of Strontium into Biomimetic Apatite. *Biomaterials* **2007**, *28*, 1452–1460. [\[CrossRef\]](#)
50. Narayanan, R.; Kwon, T.-Y.; Kim, K.-H. Direct Nanocrystalline Hydroxyapatite Formation on Titanium from Ultrasonated Electrochemical Bath at Physiological PH. *Mater. Sci. Eng. C* **2008**, *28*, 1265–1270. [\[CrossRef\]](#)
51. Ye, W.; Wang, X.X. Morphologies of Hydroxyapatite Crystal Deposited on Titanium Surface with Electrochemical Technique. *Key Eng. Mater.* **2007**, *330–332*, 601–604. [\[CrossRef\]](#)
52. Ungureanu, E.; Ionescu, I.C.; Zamfir-Andronic, R.I.; Vasilescu, M.; Milea, C.G.; Dobrescu, M.; Vranceanu, D.M.; Cotrut, C.M. Biofunctionalization of Ti6Al4V Surface with Ag Modified HAp Coatings via Electrochemical Deposition. *UPB Sci. Bull. Ser. B Chem. Mater. Sci.* **2020**, *82*, 307–324.
53. Furko, M.; Balázs, C. Morphological, Chemical, and Biological Investigation of Ionic Substituted, Pulse Current Deposited Calcium Phosphate Coatings. *Materials* **2020**, *13*, 4690. [\[CrossRef\]](#) [\[PubMed\]](#)
54. Sadat-Shojai, M.; Khorasani, M.-T.; Dinpanah-Khoshdargi, E.; Jamshidi, A. Synthesis Methods for Nanosized Hydroxyapatite with Diverse Structures. *Acta Biomater.* **2013**, *9*, 7591–7621. [\[CrossRef\]](#) [\[PubMed\]](#)
55. Uskoković, V. The Role of Hydroxyl Channel in Defining Selected Physicochemical Peculiarities Exhibited by Hydroxyapatite. *RSC Adv.* **2015**, *5*, 36614–36633. [\[CrossRef\]](#) [\[PubMed\]](#)
56. Schmidt, R.; Gebert, A.; Schumacher, M.; Hoffmann, V.; Voss, A.; Pilz, S.; Uhlemann, M.; Lode, A.; Gelinsky, M. Electrodeposition of Sr-Substituted Hydroxyapatite on Low Modulus Beta-Type Ti-45Nb and Effect on in Vitro Sr Release and Cell Response. *Mater. Sci. Eng. C* **2020**, *108*, 110425. [\[CrossRef\]](#)
57. Matsunaga, K.; Murata, H. Strontium Substitution in Bioactive Calcium Phosphates: A First-Principles Study. *J. Phys. Chem. B* **2009**, *113*, 3584–3589. [\[CrossRef\]](#)
58. Sun, J.P.; Song, Y. Strengthening Adhesion of the Hydroxyapatite and Titanium Interface by Substituting Silver and Zinc: A First Principles Investigation. *ACS Appl. Nano Mater.* **2018**, *1*, 4940–4954. [\[CrossRef\]](#)
59. Cacciotti, I. Cationic and Anionic Substitutions in Hydroxyapatite. In *Handbook of Bioceramics and Biocomposites*; Springer International Publishing: Berlin/Heidelberg, Germany, 2016; pp. 145–211.
60. Canillas, M.; Pena, P.; de Aza, A.H.; Rodríguez, M.A. Calcium Phosphates for Biomedical Applications. *Boletín De La Soc. Española De Cerámica Y Vidr.* **2017**, *56*, 91–112. [\[CrossRef\]](#)
61. Eppell, S.J.; Tong, W.; Katz, J.L.; Kuhn, L.; Glimcher, M.J. Shape and Size of Isolated Bone Mineralites Measured Using Atomic Force Microscopy. *J. Orthop. Res.* **2001**, *19*, 1027–1034. [\[CrossRef\]](#)
62. Weiner, S.; Wagner, H.D. THE MATERIAL BONE: Structure-Mechanical Function Relations. *Annu. Rev. Mater. Sci.* **1998**, *28*, 271–298. [\[CrossRef\]](#)
63. Narendran, P.; Rajendran, A.; Garhnayak, M.; Garhnayak, L.; Nivedhitha, J.; Devi, K.C.; Pattanayak, D.K. Influence of PH on Wet-Synthesis of Silver Decorated Hydroxyapatite Nanopowder. *Colloids Surf. B Biointerfaces* **2018**, *169*, 143–150. [\[CrossRef\]](#) [\[PubMed\]](#)

64. Roy, M.; Fielding, G.A.; Beyenal, H.; Bandyopadhyay, A.; Bose, S. Mechanical, In Vitro Antimicrobial, and Biological Properties of Plasma-Sprayed Silver-Doped Hydroxyapatite Coating. *ACS Appl. Mater. Interfaces* **2012**, *4*, 1341–1349. [[CrossRef](#)] [[PubMed](#)]
65. Fielding, G.A.; Roy, M.; Bandyopadhyay, A.; Bose, S. Antibacterial and Biological Characteristics of Silver Containing and Strontium Doped Plasma Sprayed Hydroxyapatite Coatings. *Acta Biomater.* **2012**, *8*, 3144–3152. [[CrossRef](#)] [[PubMed](#)]
66. Pye, A.D.; Lockhart, D.E.A.; Dawson, M.P.; Murray, C.A.; Smith, A.J. A Review of Dental Implants and Infection. *J. Hosp. Infect.* **2009**, *72*, 104–110. [[CrossRef](#)] [[PubMed](#)]
67. Wang, Q.-J.; Shen, H.; Zhang, X.-L.; Jiang, Y.; Wang, Q.; Chen, Y.S.; Shao, J.-J. Staged Reimplantation for the Treatment of Fungal Peri-Prosthetic Joint Infection Following Primary Total Knee Arthroplasty. *Orthop. Traumatol. Surg. Res.* **2015**, *101*, 151–156. [[CrossRef](#)]
68. Del Pozo, J.L.; Patel, R. Infection Associated with Prosthetic Joints. *N. Engl. J. Med.* **2009**, *361*, 787–794. [[CrossRef](#)]
69. Zhou, H.; Yang, L.; Gbureck, U.; Bhaduri, S.B.; Sikder, P. Monetite, an Important Calcium Phosphate Compound—Its Synthesis, Properties and Applications in Orthopedics. *Acta Biomater.* **2021**, *127*, 41–55. [[CrossRef](#)]
70. Kim, H.; Camata, R.P.; Lee, S.; Rohrer, G.S.; Rollett, A.D.; Hennessy, K.M.; Bellis, S.L.; Vohra, Y.K. Calcium Phosphate Bioceramics with Tailored Crystallographic Texture for Controlling Cell Adhesion. *MRS Proc.* **2006**, *925*, 0925-BB02-07. [[CrossRef](#)]
71. Wang, Y.; Liu, X.; Fan, T.; Tan, Z.; Zhou, Z.; He, D. In Vitro Evaluation of Hydroxyapatite Coatings with (002) Crystallographic Texture Deposited by Micro-Plasma Spraying. *Mater. Sci. Eng. C* **2017**, *75*, 596–601. [[CrossRef](#)]
72. Liu, X.; He, D.; Zhou, Z.; Guo, X.; Liu, Y.; Hou, W.; Li, H. In Vitro Bioactivity and Antibacterial Performances of Atmospheric Plasma Sprayed C-Axis Preferential Oriented Hydroxyapatite Coatings. *Surf. Coat. Technol.* **2021**, *417*, 127209. [[CrossRef](#)]
73. Huang, Y.; Hao, M.; Nian, X.; Qiao, H.; Zhang, X.; Zhang, X.; Song, G.; Guo, J.; Pang, X.; Zhang, H. Strontium and Copper Co-Substituted Hydroxyapatite-Based Coatings with Improved Antibacterial Activity and Cytocompatibility Fabricated by Electrodeposition. *Ceram. Int.* **2016**, *42*, 11876–11888. [[CrossRef](#)]
74. Ullah, I.; Siddiqui, M.A.; Kolawole, S.K.; Liu, H.; Zhang, J.; Ren, L.; Yang, K. Synthesis, Characterization and in Vitro Evaluation of Zinc and Strontium Binary Doped Hydroxyapatite for Biomedical Application. *Ceram. Int.* **2020**, *46*, 14448–14459. [[CrossRef](#)]
75. Stanić, V.; Janačković, D.; Dimitrijević, S.; Tanasković, S.B.; Mitrić, M.; Pavlović, M.S.; Krstić, A.; Jovanović, D.; Raičević, S. Synthesis of Antimicrobial Monophase Silver-Doped Hydroxyapatite Nanopowders for Bone Tissue Engineering. *Appl. Surf. Sci.* **2011**, *257*, 4510–4518. [[CrossRef](#)]
76. Rameshbabu, N.; Sampath Kumar, T.S.; Prabhakar, T.G.; Sastry, V.S.; Murty, K.V.G.K.; Prasad Rao, K. Antibacterial Nanosized Silver Substituted Hydroxyapatite: Synthesis and Characterization. *J. Biomed. Mater. Res. Part A* **2007**, *80*, 581–591. [[CrossRef](#)] [[PubMed](#)]
77. Jadalannagari, S.; Deshmukh, K. Antimicrobial Activity of Hemocompatible Silver Doped Hydroxyapatite Nanoparticles Synthesized by Modified Sol Gel Technique. *Appl. Nanosci.* **2014**, *4*, 133–141. [[CrossRef](#)]
78. Gittens, R.A.; Olivares-Navarrete, R.; Schwartz, Z.; Boyan, B.D. Implant Osseointegration and the Role of Microroughness and Nanostructures: Lessons for Spine Implants. *Acta Biomater.* **2014**, *10*, 3363–3371. [[CrossRef](#)] [[PubMed](#)]
79. Kunzler, T.P.; Drobek, T.; Schuler, M.; Spencer, N.D. Systematic Study of Osteoblast and Fibroblast Response to Roughness by Means of Surface-Morphology Gradients. *Biomaterials* **2007**, *28*, 2175–2182. [[CrossRef](#)]
80. Vagaská, B.; Bačáková, L.; Filová, E.; Balík, K. Osteogenic Cells on Bio-Inspired Materials for Bone Tissue Engineering. *Physiol. Res.* **2010**, *59*, 309–322. [[CrossRef](#)]
81. Zheng, S.; Bawazir, M.; Dhall, A.; Kim, H.-E.; He, L.; Heo, J.; Hwang, G. Implication of Surface Properties, Bacterial Motility, and Hydrodynamic Conditions on Bacterial Surface Sensing and Their Initial Adhesion. *Front. Bioeng. Biotechnol.* **2021**, *9*, 82. [[CrossRef](#)]
82. Evgeny, B.; Hughes, T.; Eskin, D.; Evgeny, B.T.; Hughes, D.E. Effect of Surface Roughness on Corrosion Behaviour of Low Carbon Steel in Inhibited 4 M Hydrochloric Acid under Laminar and Turbulent Flow Conditions. *Corros. Sci.* **2016**, *103*, 196–205. [[CrossRef](#)]
83. Vadgama, P. *Surfaces and Interfaces for Biomaterials*, 1st ed.; Elsevier: Amsterdam, The Netherlands, 2005; pp. 693–716.